

Biologically inspired force enhancement for maritime propulsion and maneuvering

Gabriel D. Weymouth, University of Southampton, UK,
G.D.Weymouth@soton.ac.uk

Abstract

The move to high performance applications greatly increases the demand to produce large instantaneous fluid forces for high-speed maneuvering and improved power efficiency for sustained propulsion. Animals achieve remarkable feats of maneuvering and efficiency by changing their body shape to generate unsteady fluid forces. Inspired by this, we have studied a range of immersed bodies which drastically change their shape to produce fluid forces. These include relatively simple shape-changes, such as quickly changing the angle of attack of a foil to induce emergency stops and the use of tandem flapping foils to generate three times the average propulsive force of a single flapping foil. They also include more unconventional shape-changes such as high-speed retracting foil sections to power roll and dive maneuvers and the use of soft robotics to rapidly shrink the frontal area of an ellipsoid to power 68% efficient fast-start maneuvers or even completely cancel the drag force with 91% quasi-propulsive efficiency. These systems have been investigated with analytics, experimental measurements and immersed-boundary numerical simulations.

1 Introduction

With the expansion of human activities in the oceans towards more extreme environments, state-of-the-art maritime technologies have progressively become less suited at coping with the increased degree of complexity of their missions. As an example, the offshore oil industry is more and more involved in operating in deeper waters and need to acquire baseline and on-going surveys throughout the life history of submerged infrastructures and their interaction with the surrounding ecosystems. Currently, operations of this kind rely heavily on expensive and slow human divers because traditional robots are not as well suited to acquiring in-situ measurements in very close proximity to submerged structures or living organisms.

Aerial and marine animal achieve remarkable feats of maneuvering and efficiency by changing their body shape to generate unsteady fluid forces. For example, birds execute precise maneuvers, such as banking, braking, takeoff and landing, all with minimal power expended (Provini et al., 2014). This is in stark contrast to current “flight-type” marine and aerial vehicles with fixed wings which have a fixed minimum operating speed and slow response time, or “hover-type” vehicles with multiple thrusters which have limited mission lives due to their inefficiency.

Starting with the seminal work of Lighthill (1960), which mathematically formulated how fish produce large forces and high efficiency with undulatory motion, there has been significant research in studying shape-changing unsteady biological flows and exploiting them in maritime engineering designs. While fish swimming itself has now been well studied (Triantafyllou et al., 2000) and applied to small robotic vehicles (Triantafyllou et al., 1994), the mechanical complexities make it difficult to adapt fish-propulsion to broader applications. In this manuscript, we review some recent work on biologically inspired mechanisms which generate strong forces, are highly efficient, and are achieved with relatively simple actuation methods, all of which makes them potentially well-suited to maritime applications.

2 Heaving and pitching foils

The first biologically inspired force-producing device was certainly a flapping wing, dating at least as far back as Da Vinci ca. 1485 (McCurdy et al., 1941). Modern research has revitalized this concept, showing that lifting surfaces which are actuated to dynamically heave and/or pitch have potential advantages over either fixed lifting surfaces or standard propellers. Studies on the thrust forces generated by an oscillating foil have shown the potential for impressive thrust coefficients (maximum of $C_T = 2.4$) and efficiency regions of 50-60% (Read et al., 2003). It has also been shown that an oscillating foil can be

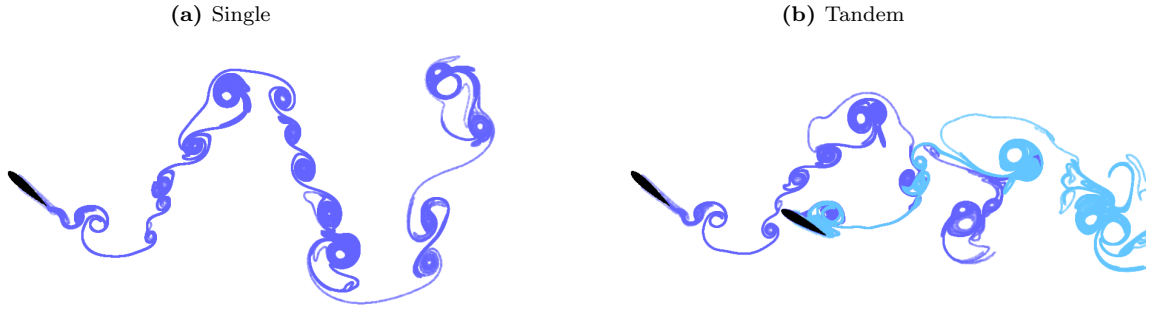


Figure 1: Simulated streaklines for the two-dimensional flow past a single flapping foil and tandem flapping foils. The streaklines are visualized by continuously releasing tracer particles on either side of the foil at the quarter-chord. The tandem case has phase lag $\phi = 1.75\pi$, and spacing $s = 2c$.

used to manipulate incoming vorticity for energy extraction, with efficiencies at and above 45% (Simpson et al., 2008). However, there are a wide range in observed efficiencies and force magnitudes, and these parameters vary with oscillation type, planform and flexibility of the foil. This section reviews two studies on actuated rigid foils which demonstrate large force production at high efficiency levels with simple kinematics.

2.1 Tandem flapping foils to balance forces and utilize wake energy

A fundamental issue with implementing a flapping foil as a marine propulsor on an otherwise conventional ship or underwater vehicle is the large variation in thrust and side force. Additionally, propulsive efficiency in the range of 50-60% is not optimum, indicating that mechanical power is being wasted in energizing the wake. A recent study by Epps et al. (2016) investigated the use of tandem flapping foils to mitigate the unbalanced forces and potentially increase efficiency by utilizing energy in the wake of the forward foil.

In this study, the foils undergo prescribed harmonic heave h and pitch θ , defined as

$$h_f(t) = c \sin(\omega t), \quad h_b(t) = c \sin(\omega t + \phi) \quad (1)$$

$$\theta_f(t) = \frac{\pi}{4} \cos(\omega t), \quad \theta_b(t) = \frac{\pi}{4} \cos(\omega t + \phi) \quad (2)$$

where c is the chord length, ω is the flapping frequency and ϕ is the phase lag between the foils, and the f, b subscripts refer to the front and back foils respectively. The frequency is set to achieve a Strouhal number of $St = 4\pi\omega c/U = 0.4$, known to be at the upper end of the range resulting in high thrust for a single foil (Read et al., 2003). The flow speed U is set to achieve a Reynolds number of $Re = Uc/\nu = 10^4$.

This flow was studied using the Lily Pad computational fluid dynamics software. As discussed in Weymouth (2015), Lily Pad is a two-dimensional Cartesian-grid flow solver that uses the Boundary Data Immersion Method (see Maertens and Weymouth, 2015) and has been extensively validated for unsteady fluid-body interaction problems. For these simulations, a grid spacing of $h = c/64$ and a domain size of $16c \times 8c$ was used.

Figure 1 shows a set of Lily Pad results for the flow around single and tandem flapping foils. Streaklines in Figure 1a show that the characteristic reverse Kármán street has formed, accelerating the flow behind the single foil. Figure 1b shows a set of streaklines for a tandem case where the leading edge of the back foil is spaced $s = 2c$ behind the trailing edge of the front foil and the motion is lagged by $\phi = 1.75\pi$. The wake in the tandem case has narrowed and lengthened compared to the single foil case, indicating greater speed and possibly efficiency.

A set of performance metrics are shown in Figure 2. The thrust T and lift L are defined as the integrated fluid force inline with and perpendicular to the oncoming flow, as usual. The general equation for the power transferred from the body to the fluid is

$$P = \oint_S \left(\vec{f}(s, t) \cdot \vec{u}(s, t) \right) ds \quad (3)$$

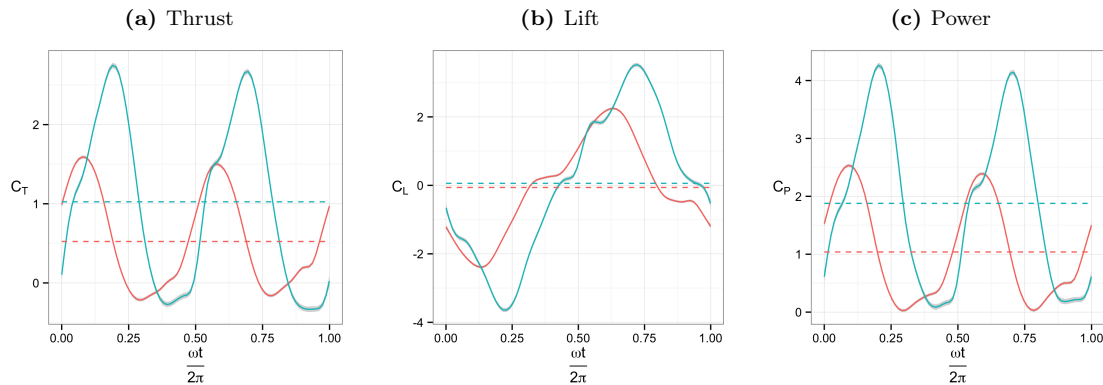


Figure 2: Performance coefficients for the tandem foils shown in Figure 1b; **front foil**, **back foil**; dashed lines are the mean values over the cycle.

where \vec{f} is the local fluid force per unit area on the body surface, \vec{u} is the local body surface velocity, $\oint_S ds$ is an integral over the body surface. This formula automatically accounts for both the pitch and heave motion and is also valid for the flexible and deforming bodies used in the next sections.

Another key performance metric is the efficiency, which is *the rate of useful work done per unit power consumed*. As such, the hydrodynamic efficiency of a propulsive actuator operating at a steady forward speed is simply

$$\eta_t = \frac{TU}{P} \quad (4)$$

where TU is the rate of work done in the inline direction.

The results in Figure 2 are for the tandem case, but the performance of the front foil is essentially independent of the back foil for $s > c$. The front foil results compare well to those presented in the literature for single flapping foils, with a mean thrust coefficient of $C_{T,f} = T_f / (\frac{1}{2}\rho U^2 c) = 0.52$, mean lift of zero, and mean power coefficient of $C_{P,f} = P_f / (\frac{1}{2}\rho U^3 c) = 1.04$. Therefore the efficiency for this simple choice of kinematics is 50%.

The back foil undergoes the same motion as the front, but operates in its wake, which significantly changes the response. Most noticeable is the large increase this enables in the back foil thrust, $C_{T,b} = 1.02$, twice the value of the front foil. In other words, adding a second foil has not doubled the total thrust, but instead tripled it. This is due to the positive wake interference of the two foils. Negative interference is also possible, and Epps et al. (2016) develops a relationship between the spacing and phase to characterize this interference.

In addition, the peak forces on the hind foil are phase shifted by ϕ relative to the front foil. By properly setting the spacing and phase, Epps et al. (2016) shows that a tandem foil propulsion system would be capable of greatly reducing the variation in the thrust force compared to a single flapping foil. It is also possible to reduce the variation in lift, but because the thrust peaks are twice as frequent, two foils cannot perfectly cancel both thrust and lift variation.

Finally, the increased thrust on the back foil shown in Figure 2 does require increased power, but not disproportionately. In fact, the efficiency of the tandem foil system overall is $\eta_t = 53\%$, slightly better than that of the front foil alone.

2.2 Rapid pitch-up for impulsive stopping force

One of the most striking advantages of flying animals over fixed-wing aircraft is their ability to come to a complete and controlled landing in only a few body lengths; even large gliding birds such as an eagle (Carruthers et al., 2007). Like aircraft, flight-type underwater vehicles have a minimum operating speed to maintain their depth, and because maritime vessels are proportionally much heavier than aircraft, they are even slower to stop. Polet et al. (2015) studied a simple model of wing kinematics during perching and found that very large dynamic lift and drag forces are produced - and these forces could potentially be utilized to impulsively stop heavy and streamlined maritime vehicles.

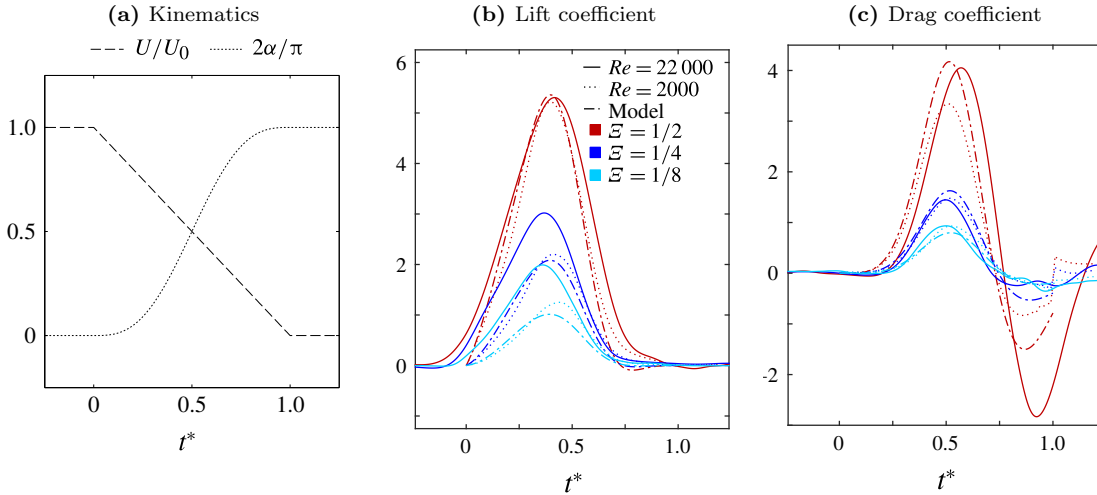


Figure 3: Kinematics and force coefficients (scaled by U_0) on a foil with rapidly increasing pitch during deceleration, reproduced from Polet et al. (2015). The force coefficients from two-dimensional simulations at $Re = 2000$, experiments at $Re = 22000$, and an inviscid flow model are given over three maneuver speeds.

Polet et al. (2015) focused on one key kinematic characteristic of bird perching, the rapid increase in pitch of the wings during deceleration. Lily Pad simulations ($Re = 2000$) and experiments ($Re = 22000$) were performed in which the foil speed and pitch angle were varied during the maneuver as

$$U(t) = U_0(1 - t^*) \quad (5)$$

$$\theta(t) = \theta_{final} \left(t^* - \frac{\sin(2\pi t^*)}{2\pi} \right) \quad (6)$$

where U_0 is the initial velocity, $\theta_{final} = \frac{\pi}{2}$ is the final pitch position, and $t^* = t/\tau$ is time scaled by the period of the maneuver τ up to $\theta = \pi/2$. A NACA0012 foil section was used and the center of rotation was set $c/6$ from the leading edge.

We quantify the impulsiveness of the maneuver using the shape-change number

$$\Xi = V/U_0 \quad (7)$$

where V is the speed of the shape-change (Weymouth and Triantafyllou, 2013). For this maneuver we choose $V = c/\tau$, the average cross-flow velocity of the trailing edge.

Figure 3 shows the resulting forces from the simulations, experiments, and an inviscid flow model described in Polet et al. (2015). Forces increased with increasing shape-change number, and at $\Xi = 1/2$ the values are ten times larger than the lift and drag at the corresponding static pitch angle, which would help birds maintain lift and come to a controlled stop. However, the drag forces are negative at the end of the maneuver which decreases the average stopping force. Polet et al. (2015) postulate that the unwanted thrust generation is due to the prescribed constant rate of deceleration in equation 10, which does not match the natural fluid-structure interaction in true perching.

To test this theory and to determine the applicability of pitching foils on maritime vehicles we next carry out free-running simulations of a stopping maneuver. The vehicle is set to be a neutrally buoyant ellipsoid with uniform density, diameter c and length $8c$, Figure 4. A NACA0012 foil with span s is mounted on either side of the body center and the pitch relative to the body is given by equation 6. We set $Re = U_0 c/\nu = 22000$. The dynamics of the vehicle are modeled as

$$\ddot{x} = \frac{D - \frac{1}{2}C_x\rho A_x\dot{x}|\dot{x}|}{m + m_{xx}}, \quad \ddot{y} = \frac{L - \frac{1}{2}C_y\rho A_y\dot{y}|\dot{y}|}{m + m_{yy}}, \quad \ddot{\psi} = \frac{M}{I + m_{\psi\psi}} \quad (8)$$

where x, y are the body centroid location, ψ is the heading, m is the mass, I is the moment of inertia, and C_a, A_a, m_{aa} are the drag coefficient (taken from Hoerner, 1965), projected area, and potential flow

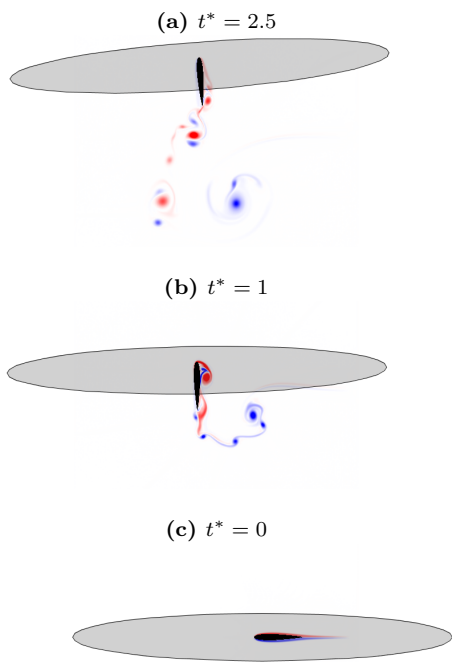


Figure 4: Foil vorticity field for free-running simulations of an ellipsoid undergoing a stopping maneuver by rapidly pitching foils with $\Xi = 1/2$, $\theta_{final} = \pi/2$.

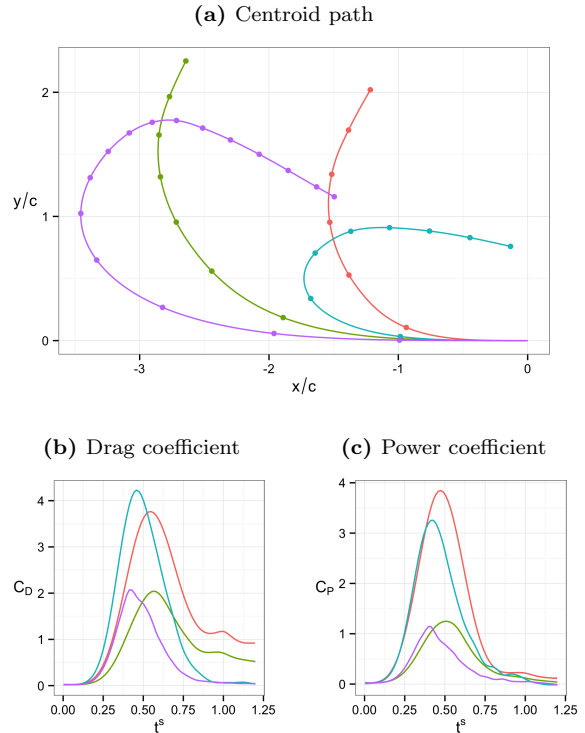


Figure 5: Results for four stopping maneuver cases; $\{\Xi, \theta_{final}\} = \{1/2, \pi/2\}, \{1/4, \pi/2\}, \{1/2, \pi\}, \{1/4, \pi\}$. Points in (a) show increments of $tU_0/c = 1$.

added-mass in the a -direction. Note that while the fluid forces on the body are modeled analytically, D, L, M are the measured lift drag and moment of the foil in the coupled simulation.

The results of the maneuvering simulations are shown in Figure 5. Increasing the shape-change rate increases the forces, and the peak drag magnitudes are similar to the prescribed deceleration case results in Figure 3. However, the free-running case results in only positive drag force, verifying the Polet et al discussion, and helping the vehicle stop. The resulting trajectories show that the pitch-up maneuver is capable of stopping the body’s forward motion in $1.6c$, only 20% of the body length.

Figure 5 also shows two cases where the final pitch has been increased to π in equation 6, e.g. the foil keeps pitching until it faces backwards. This motion ensures that it is the dynamic forces responsible for stopping the body - not just bluff-body drag on the sideways foil. The results show the body not only stops, but fully reverses, and does so with relatively little vertical drift.

3 Size and shape-changing bodies

In contrast to rigid body kinematics, such as flapping, little research has been devoted to explosive size and shape-change despite its prevalence in nature. For example, many animals use “burst and coast” gaits when performing maneuvers to reduce the cost of transport by as much as 50% (Weihs and Webb, 1984; Chung, 2009). Extreme shape change is also often used in “survival” hydrodynamics, i.e. to help an animal hunt or evade attack where extreme accelerations are required (Triantafyllou et al., 2016).

In this section we review two series of recent studies on using size-change as a novel form of force generation. Surprisingly, the ‘ballistic’ nature of these novel actuation methods often makes them simpler to implement than the controlled kinematics of the previous section. And advances in soft-robotics are enabling the first tests of these size-and shape changing devices.

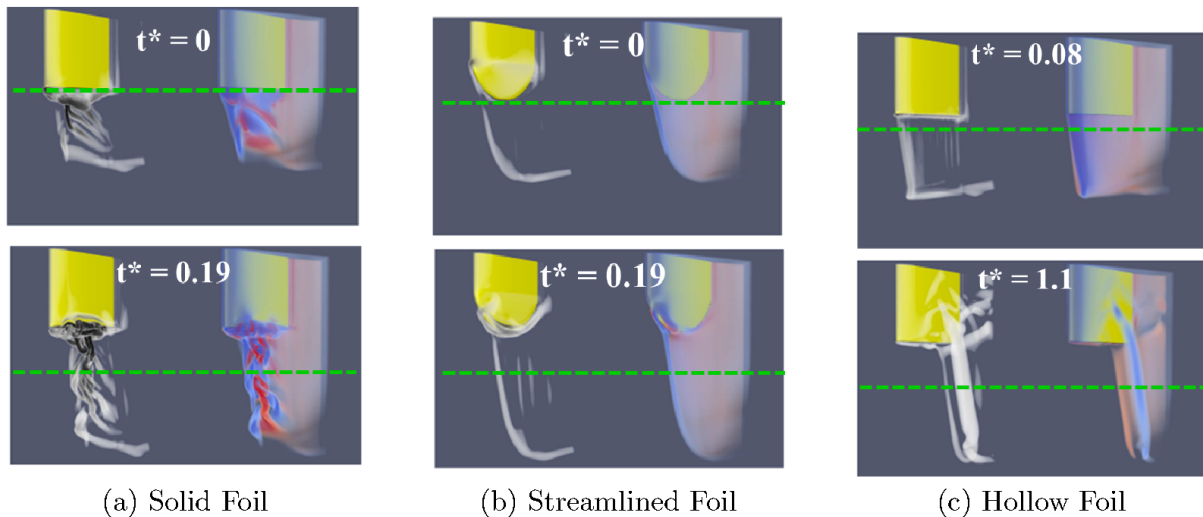


Figure 6: Simulations of the retracting foil at $Re = 1000$ for three foil geometries. $t^* = tU/c = 0$ is when the foil crosses the PIV plane (green line). The left and right of each panel show λ_2 and ω_z iso-surfaces, respectively. Reproduced from Steele et al. (2016).

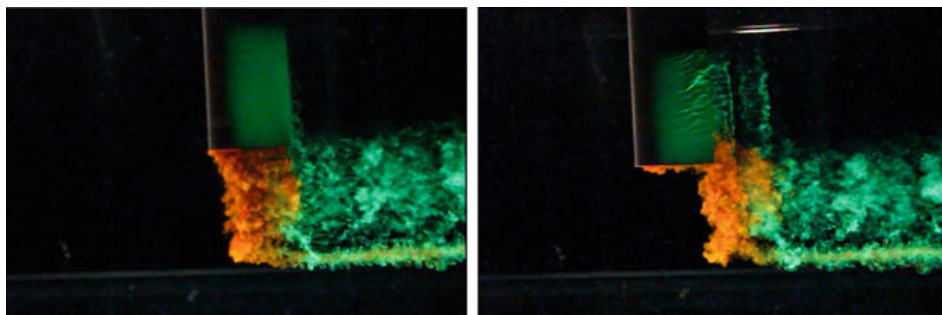


Figure 7: Experiment with dye injection of the retracting open hollow foil at $Re = 13700$. The orange dye is from inside the foil, while the green is from the outside. The left image is around $t^* = 0.15$, right is around $t^* = 1.15$. Reproduced from Steele et al. (2016).

3.1 Span-wise retraction to shed vorticity

When birds and marine mammals perform “burst and coast” maneuvers they rapidly pull their wings or flippers against their bodies - causing them to effectively ‘vanish’ from the flow. Classic studies such as Taylor (1953) showed that this sudden disappearance would leave a significant vortex in the fluid, generating large forces. Wibawa et al. (2012) attempted to experimentally and numerically study this vanishing phenomenon by quickly retracting a foil along its span while towing it forward. Retraction is much simpler and less power-consuming than flapping and could be easily used in practical maritime designs.

The study used a foil with a rectangular planform, square tip, and NACA0012 cross-section. The foil was towed along the tank at $Re = Uc/\nu = 14000$ at a 10 deg angle of attack and was retracted a distance $1.4c$ with an average speed of $6U$. Experimental results showed that while some circulation was shed, it was less than half of the bound circulation before retracting, and it decayed so quickly that it couldn’t be feasibly used to generate maneuvering forces.

Three-dimensional simulations were performed to visualize the complete flow. Figure 6(a) shows a similar simulation, but run at $Re = 1000$ to clarify the vorticity structures. The wake structures were found to be highly complex because the impulsive retraction of the foil generated its own wake, which mixed and disturbed the shedding of the bound vorticity. Again, this limits the amount of useful work that the maneuver can achieve.

In a follow-up study, Steele et al. (2016) showed that the shape of the foil geometry can be easily

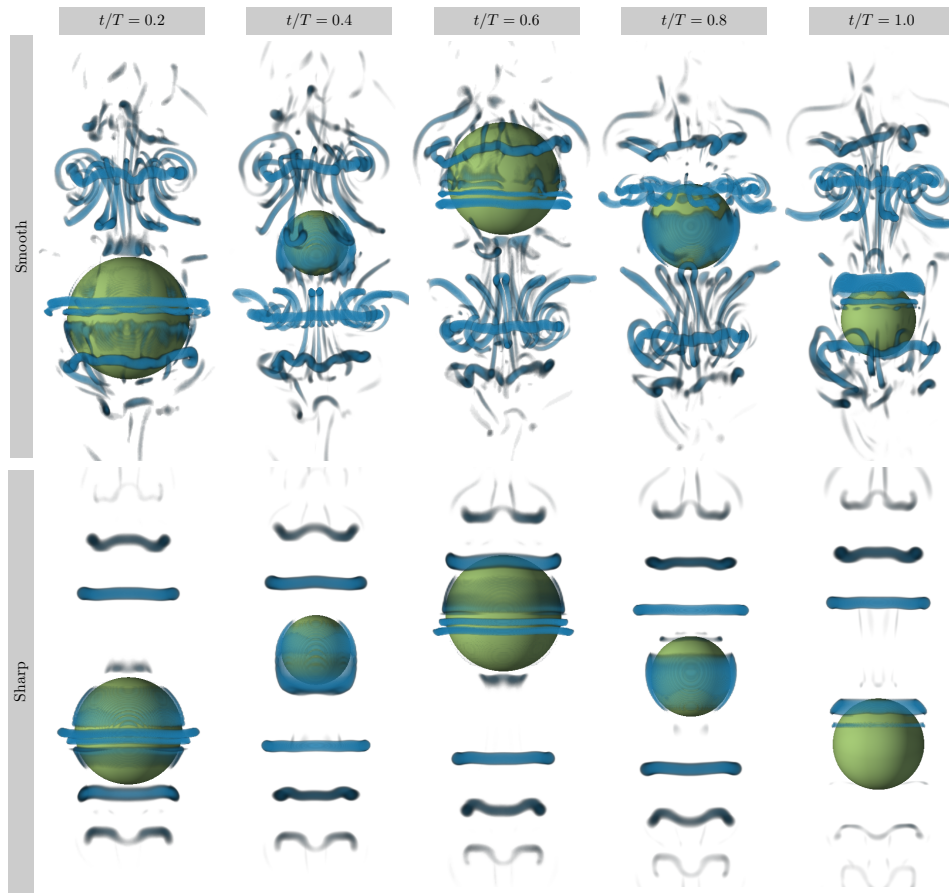


Figure 8: Evolution of the λ_2 vortex criterion during one oscillation after attainment of zero-damping regime in response to the sharp and smooth radius variations (see Figure 9). Reproduced from Giorgio-Serchi and Weymouth (2016).

adjusted to achieve different kinds of fluid response. Figure 6 shows the result of the same retraction maneuver on two other foil shapes; a foil with a streamlined and rounded wing tip, and a foil which is hollow and open on the wing tip to allow fluid to pass through. Figure 7 shows the result of using dye visualization in an experimental test of the retracting hollow foil. The results show that because the hollow foil does need to pull fluid up to fill the wake of its retraction, the vorticity is shed in two large clear vortex structures which could be used to induce dynamic roll moments on trailing control surfaces.

3.2 Shrinking to recover added-mass energy and cancel drag

The streamlined foil result in Figure 6 is entirely different than that of the hollow foil. Consider the cross-section of the streamlined foil as it retracts through the PIV plane. This is not a ‘vanishing’ body, but a shrinking one. The key difference, as shown in Weymouth and Triantafyllou (2012), is that the shrinking body pulls in fluid to fill the void left by its retraction, while a vanishing hollow body does not.

In both cases, the reduced size of the body means a corresponding reduction in the fluid added-mass. However, the resulting dynamics of the fluid, and its force on the body could not be more different. For a vanishing body, the surplus fluid kinetic energy goes into the generation of shed vortical structures as shown in Figure 6(c). For a shrinking body, two related effects were found:

1. The rapid motion of the boundary generates a layer of vorticity which can cancel the boundary layer vorticity for high shape-change numbers. This is demonstrated by the small amount of shed vorticity in Figure 6(b).
2. The cancellation of bound vorticity enables the transfer of the fluid added-mass energy back into the body, resulting in significant instantaneous forces.

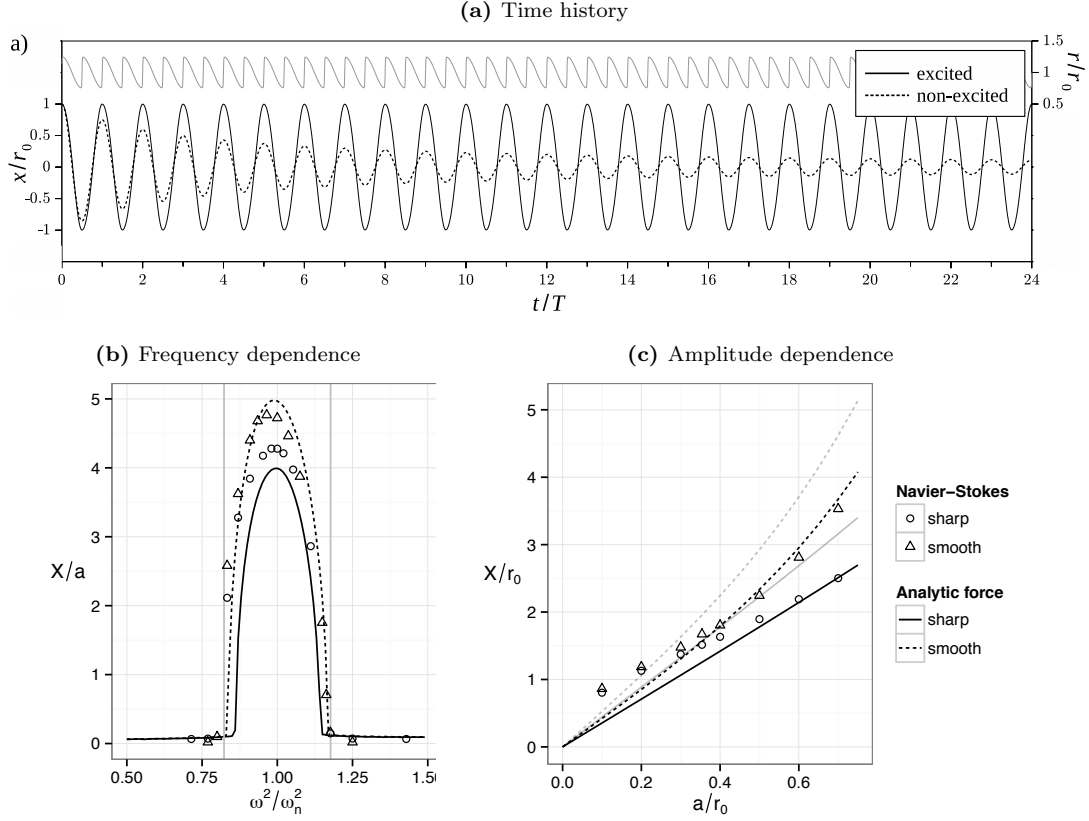


Figure 9: Transverse response x of the oscillating sphere, with and without volume-change excitation. Sharp excitation refers to the ‘saw tooth’ pattern at the top of (a), while smooth excitation is a simple sin wave pattern. The grey lines in (c) assume 100% efficient added-mass energy recovery, while the dark lines assume $\eta = 0.9$. Reproduced from Giorgio-Serchi and Weymouth (2016).

In the case of an inviscid fluid, the bound vorticity cancellation is perfect, and the resulting force is simply

$$F = -\frac{\partial}{\partial t} (m_{xx}U) = -\dot{m}_{xx}U - m_{xx}\dot{U} \quad (9)$$

where \dot{m}_{xx} is the rate of change of the added-mass. The final term is the standard added-mass force due the body acceleration, but the first term is due to the recovery of added-mass energy by the body. For large shape-change numbers $\dot{m}_{xx}U$ could be sufficient to completely cancel the body drag force.

Giorgio-Serchi and Weymouth (2016) used a volume-changing oscillator to test this method of drag cancellation. They simulated the flow on a spherical body with radius r connected to a spring and immersed in water. If this body is released from a large displacement, say $x_0 = r$, it will oscillate with a natural frequency ω_n but the amplitude will quickly decays to nothing due to the drag of the fluid, Figure 9(a, non-excited). However, if the radius of the sphere changes in time with amplitude a , then added-mass energy will transfer back and forth between body and fluid, exciting oscillation, Figure 8 and 9(a, excited).

This is called a parametric-oscillator, and just like a child on a swing changing their center of effort, this can lead to sustained large amplitude oscillations if the oscillator is pumped near the natural frequency. But while a swing would work underwater, the amplitude would be tiny due to drag. By shrinking and growing, the sphere’s large bluff body drag force is canceled, enabling oscillation amplitudes up to $X = 4.7a$ and $3.5r_0$, Figure 9.

Figure 9 also compares the results to an analytic parametric-oscillator model developed in Giorgio-Serchi and Weymouth (2016) using equation 9. While the frequency match is excellent, the model over predicts X for large a because of the imperfect recovery of added-mass energy. Indeed, Figure 8 shows the simulated flow features large scale vortex shedding - indicating that at least some portion of the energy is spent stirring up the fluid.

To quantify how much energy is wasted, we need to revisit the definition of efficiency. Unlike for an isolated propulsor, the useful work is ill-defined for a self-propelled body. As discussed in Maertens et al. (2015) this is because the net force on a steady self-propelled body is zero by definition and the power lost to the environment depends sensitively on the propulsion method. Instead, we must use the quasi-propulsive efficiency

$$\eta_{QP} = \frac{P_{tow}}{P_{self}} \quad (10)$$

where P_{tow} is the power lost to the fluid when *towing the rigid body at its operating condition*, and P_{self} is the power usage measured in the self-propelled test.

This is, in fact, the standard measure of efficiency used in ship design. In the case of a propeller-driven ship at steady-ahead conditions equation 10 becomes

$$\eta_{QP} = \frac{RU}{Q\omega} \quad (11)$$

where the towed resistance R times the speed U is the towed power loss, and the propeller shaft torque Q times the rotation rate ω is the self-propelled power usage. When using equation 10, the towed body should be rigid and bare (no propulsor) but otherwise operated at the same conditions as the self-propelled test.

Applied to the case of the volume-changing and oscillating sphere, we first select a self-propelled case, say $a/r_0 = 0.35$ and $\omega = \omega_n$ which achieved in $X/a = 4.7$ using the smooth profile. We then repeat this case with a rigid sphere towed at the same frequency and amplitude of motion. After using equation 3 to measure the power used in both cases, the quasi-propulsive efficiency is found to be $\eta_{QP} = 0.91$. This was found to be a representative value for the resonant smooth profile cases.¹ Using this value, the analytic prediction can be corrected and agrees well with experiments, Figure 9.

If drag cancellation with 90% efficiency seems too good to be true, it may be explained (or perhaps rationalized) by considering that the growing and shrinking of a shape in water induces a completely irrotational fluid motion. Unlike the rotation of a propeller or flapping of a foil then, an inflate-deflate cycle is perfectly reversible, resulting in a zero net transfer of energy to the fluid over the cycle. As the maturing field of soft robotics enables designs with highly deformable parts (Giorgio-Serchi et al., 2013), such efficiencies may be soon be realized experimentally.

3.3 Deflating to power an ultra-fast start

Cephalopods, such as the squid and octopus, greatly increase their size by filling with water, before ejecting the water in a propulsive jet, reducing their size and helping them make a quick escape (Huffard, 2006). As a final example of biologically inspired-force production, we review a series of studies that investigated a jet-propelled shrinking vehicle as a model of this system both analytically and experimentally.

Weymouth and Triantafyllou (2013) consider three types of jet-propelled bodies; a rocket in the vacuum of space, a rigid 5:1 ellipsoidal torpedo in water, and an octopus-like vehicle which shrinks from a sphere to a 5:1 ellipsoid as it jets. The acceleration of all three is governed by the simple equation

$$\ddot{x} = \frac{F - \dot{m}U_J}{m} = \frac{\sum F}{m} \quad (12)$$

where $\sum F$ is the total force, which is the fluid force F plus the jet thrust $T_J = -\dot{m}U_J$, $-\dot{m}$ is the rate of mass loss and U_J is the jet exit velocity.

Figure 10 shows the results for all the three cases when jetting from rest until 96% of the initial mass m_0 has been expelled, keeping U_J constant for the majority of the maneuver.

- In a vacuum, $F = 0$ and the net force $\sum F$ equals T_J . The rocket accelerates at an increasing rate due to decreased inertia, accelerating far beyond the jet velocity.
- If we model the fluid reaction force on the rigid torpedo with equation 9, then the body experiences no drag, but will have an ever increasing added-mass force such that $\sum F \ll T_J$. In essence, the torpedo's added mass is an additional payload which it never sheds, limiting its acceleration.

¹ Note that the power transfer during sharp inflation is infinite, making this a rather poor choice for energy efficiency. Even use a slightly smoothed profile, the extreme magnitude of the power peaks made computing a meaningful average impossible.

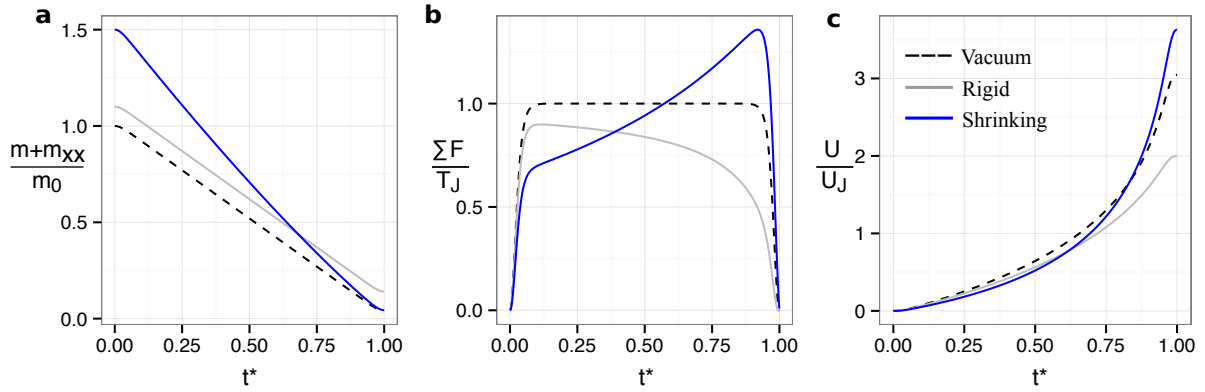


Figure 10: Comparison of three jet-propelled rocket fast-start maneuvers using equation 9 to model the fluid reaction force.

- The octopus-like vehicle starts as a sphere, meaning its inertia is initially 50% greater than the rocket in space. However, unlike the rigid torpedo, this is not payload - it is additional propellant! As the body shrinks, the added-mass energy is recovered in the form of thrust by equation 9. In the second half of the maneuver, when the inertia is reduced, this results in $\sum F \gg T_J$.

The final result being that the octopus-like body accelerates to speeds above $3.5U_J$, much faster than the rigid torpedo, and even faster than a rocket in the vacuum of space.

As discussed above, the successful recovery of added-mass energy requires that the energy is not lost to shed vorticity. Weymouth et al. (2015) studied this process and developed an analytic parameter to predict the recovery efficiency. As the octopus-like vehicle shrinks, it induces a normal velocity which draws in the boundary layer fluid. If this inward velocity is strong enough to overcome the diffusion of the boundary layer, then the vorticity can be annihilated and the flow energy recovered. Weymouth et al. (2015) liken this to the application of suction on a rigid boundary layer. In analogy to a suction parameter, they define a shrinking parameter

$$\sigma^* = V \sqrt{\frac{L}{U\nu}} = \Xi \sqrt{Re} \quad (13)$$

where V is the cross-flow velocity of the deforming body, in this case the rate of change of the minor-axis radius. This modification of the shape-change number includes the rate of boundary layer diffusion, and axis-symmetric boundary layer theory suggests that $\sigma^* > 9$ should be a threshold value for delayed separation and energy recovery. Note that this threshold is easier to achieve at larger Reynolds numbers, and therefore large body-sizes.

Based on this, Weymouth et al. (2015) designed a prototype soft robotics vehicle to maximize σ^* during a jet-propelled fast start maneuver. The octopus-inspired vehicle consists of a rigid neutrally buoyant skeleton with an elastic membrane stretched around it to form the outer hull, Figure 11(a). As with the mantle of the octopus, this membrane can be inflated, giving it an initially bluff shape and storing sufficient energy to power its escape. The fully deflated hull shape is approximately a 5:1 ellipsoid, and is sufficiently streamlined to allow the body to coast dozens of body lengths. The body length is $L = 26\text{cm}$ and the volume when fully deflated is 1030cm^3 , so the ‘payload’ mass accelerated by the maneuver is $m_f = 1.03\text{ kg}$.

Once inflated, the robot is released from a mount allowing it to accelerate forward in open water under its own power. The resulting fast-start maneuver performance is measured using high-speed cameras at 150 frames/second. Figure 11 shows the rapid acceleration and deflation of the shrinking robot from a self-propelled run. The velocity peaks above 10L/s or 2.7m/s around $t = 0.95\text{s}$ after release. Based on this and scale of deformation of the body we have $\Xi_{ave} = 1/24$, $Re_{ave} = 350000$ and the shrinking parameter is $\sigma^* > 77$ throughout the maneuver, well above the threshold.

This high shrinking parameter indicates we should have efficient energy recovery. To quantify this the outline of the body is measured from the images to determine the mass, mass flux, net force ($m\ddot{x}$), and

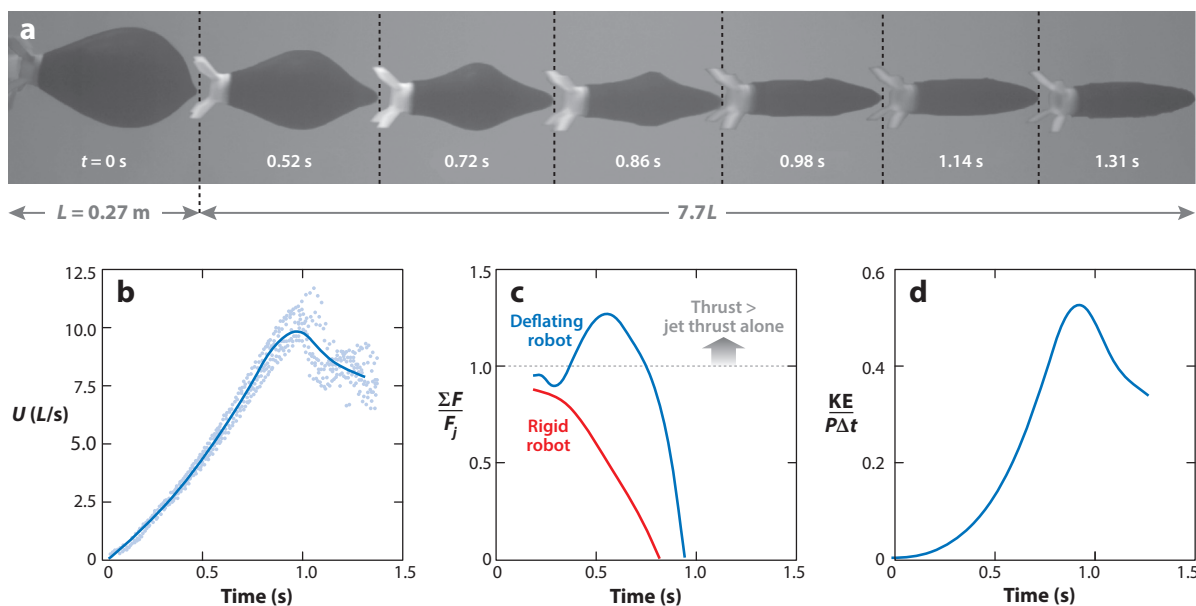


Figure 11: Results of the self-propelled test of the octopus-inspired vehicle. Reproduced from Triantafyllou et al. (2016), where $F_j = T_j$ is the jet thrust.

jet thrust ($-mU_J$) during the maneuver. Figure 11 shows that the peak net force is 30% greater than T_J , similar to the analytic predictions.

We can also measure the payload kinetic energy and the integrated power delivered by the jet:

$$KE = \frac{1}{2}m_f U^2, \quad P\Delta t = \frac{1}{2} \int_0^\tau \dot{m} U_J^2 dt \quad (14)$$

Figure 11 shows the ratio of these values, which peaks at 53%. This is on par with the theoretical propulsive efficiency of rocket accelerating from rest in a vacuum, which peaks at 65% (Ivey, 1947).

However, this is *not* the quasi-propulsive efficiency of the prototype. The integrated P_{tow} is the change in kinetic energy **plus** the integral of RU when towing the deflated body through the same maneuver. Using the conservative values $C_D = 0.05$ and $m_{xx} = m_f/10$ for the deflated shape gives a quasi-propulsive efficiency of $\eta_{QP} = 68\%$, better than a rocket in space.

4 Discussion and Conclusions

Vorticity generation is the key to all fluid force generation. It is text-book knowledge that increasing the speed of a body will generally generate more vorticity and increase the force. Slightly less well known is that added-mass in a viscous fluid is also based on vorticity generation on the body surface, making this a unifying theme in fluid dynamics (Wu et al., 2007).

In this context, one characteristic stands out in the biological-inspired studies above:

Unsteady biologically-based propulsors optimize the generation of vorticity by coordinating their kinematics and shape-change with the state of the flow.

The additional degrees of freedom in biologically-based systems gives them the potential to generate vorticity when and where it will be most useful, and this can be utilized to efficiently produce large forces for maritime applications.

- In the case of tandem flapping foils, proper phase and distance gaps between the foils enable positive interference to double the thrust on the back foil, or to reduce the variation in lift and thrust.
- A foil pitched-up rapidly is capable of generating large vorticity if the shape-change number Ξ is increased, and can bring a streamlined body to a complete stop in 20% of its length.

- Spanwise-retraction of a hollow foil minimizes the generation of new vorticity, freeing the bound vorticity to do other useful work.
- On the other hand, retracting a foil with a streamlined planform generates opposite-sign vorticity on the boundary, annihilating the bound vorticity.
- This annihilation enables a body to recover the fluid's added-mass kinetic energy in the form of a large unsteady force. If timed with the natural frequency, this can be used to cancel drag on a size-changing sphere with 91% efficiency.
- Finally, by treating the added-mass as additional propellant, stored up initially and released throughout, a shrinking underwater vehicle can achieve an ultra-fast start.

This recovery of fluid energy in the form of thrust is especially interesting, and occurs readily as long as its shrinking rate σ^* overcomes viscous diffusion. As this number increases with Reynolds number, even greater quasi-propulsive efficiency may soon be realized experimentally.

Acknowledgements

This work was performed in collaboration with excellent research groups world-wide; including Michael Triantafyllou's group at MIT, David Rival's group at Queens University, Brenden Epp's group at Dartmouth University, and Bharathram Ganapathisubramani's group at University of Southampton.

References

- Anna C Carruthers, Adrian LR Thomas, and Graham K Taylor. Automatic aeroelastic devices in the wings of a steppe eagle aquila nipalensis. *Journal of Experimental Biology*, 210(23):4136–4149, 2007.
- MH Chung. On burst-and-coast swimming performance in fish-like locomotion. *Bioinspiration & biomimetics*, 4(3):036001, 2009.
- Brenden P Epps, Luke E Muscutt, Bernard T Roesler, Gabriel D Weymouth, and Bharathram Ganapathisubramani. On the interfoil spacing and phase lag of tandem flapping foil propulsors. *Journal of Ship Production and Design*, 2016.
- F. Giorgio-Serchi and G. D. Weymouth. Drag cancellation by added-mass pumping. *Journal of Fluid Mechanics*, 798, Jun 2016. doi: 10.1017/jfm.2016.353. URL <http://dx.doi.org/10.1017/jfm.2016.353>.
- Francesco Giorgio-Serchi, Andrea Arienti, and Cecilia Laschi. Biomimetic vortex propulsion: toward the new paradigm of soft unmanned underwater vehicles. *IEEE/ASME Transactions On Mechatronics*, 18(2):484–493, 2013.
- Sighard F Hoerner. *Fluid-dynamic drag: practical information on aerodynamic drag and hydrodynamic resistance*. Hoerner Fluid Dynamics Midland Park, NJ, USA, 1965.
- C. L. Huffard. Locomotion by *abdupus aculeatus* (cephalopoda: Octopodidae): walking the line between primary and secondary defenses. *J. Expl. Biol.*, 209:3697–3707, 2006.
- H Reese Ivey. Letter to editor. *Journal of the Aeronautical Sciences*, 14(8):450–450, 1947. doi: 10.2514/8.1409. URL <http://dx.doi.org/10.2514/8.1409>.
- MJ Lighthill. Note on the swimming of slender fish. *Journal of fluid Mechanics*, 9(02):305–317, 1960.
- AP Maertens, MS Triantafyllou, and DKP Yue. Efficiency of fish propulsion. *Bioinspiration & Biomimetics*, 10(4), 2015.
- Audrey P Maertens and Gabriel D Weymouth. Accurate cartesian-grid simulations of near-body flows at intermediate reynolds numbers. *Computer Methods in Applied Mechanics and Engineering*, 283:106–129, 2015.

- Edward McCurdy et al. *The notebooks of Leonardo da Vinci*. Garden City publishing co., inc., 1941.
- Delyle T. Polet, David E. Rival, and Gabriel D. Weymouth. Unsteady dynamics of rapid perching manoeuvres. *Journal of Fluid Mechanics*, 767:323–341, 2015. doi: 10.1017/jfm.2015.61.
- P. Provini, B. W. Tobalske, K. E. Crandell, and A. Abourachid. Transition from wing to leg forces during landing in birds. *J. Exp. Biol.*, 2014. doi: 10.1242/jeb.104588. URL <http://jeb.biologists.org/content/early/2014/05/08/jeb.104588.abstract>.
- Douglas A Read, FS Hover, and MS Triantafyllou. Forces on oscillating foils for propulsion and maneuvering. *Journal of Fluids and Structures*, 17(1):163–183, 2003.
- Bradley J Simpson, Stephen Licht, Franz S Hover, and Michael S Triantafyllou. Energy extraction through flapping foils. In *ASME 2008 27th International Conference on Offshore Mechanics and Arctic Engineering*, pages 389–395. American Society of Mechanical Engineers, 2008.
- S.C. Steele, J.M. Dahl, G.D. Weymouth, and M.S. Triantafy. Shape of retracting foils that model morphing bodies controls shed energy and wake structure. *Journal of Fluid Mechanics*, to appear, 2016.
- GI Taylor. Formation of a vortex ring by giving an impulse to a circular disk and then dissolving it away. *Journal of Applied Physics*, 24(1):104–104, 1953.
- M. S. Triantafyllou, G. S. Triantafyllou, and D. K. P. Yue. Hydrodynamics of fishlike swimming. *Annual Review of Fluid Mechanics*, 32(1):33–53, 2000. doi: 10.1146/annurev.fluid.32.1.33. URL <http://www.annualreviews.org/doi/abs/10.1146/annurev.fluid.32.1.33>.
- Michael S. Triantafyllou, Gabriel D. Weymouth, and Jianmin Miao. Biomimetic survival hydrodynamics and flow sensing. *Annual Review of Fluid Mechanics*, 48(1):null, 2016. doi: 10.1146/annurev-fluid-122414-034329. URL <http://dx.doi.org/10.1146/annurev-fluid-122414-034329>.
- MS Triantafyllou, MA Grosenbaugh, and R Gopalkrishnan. Vortex-induced vibrations in a sheared flow: a new predictive method. Technical report, DTIC Document, 1994.
- D Weihs and Paul W Webb. Optimal avoidance and evasion tactics in predator-prey interactions. *Journal of Theoretical Biology*, 106(2):189–206, 1984.
- G D Weymouth. Lily pad: Towards real-time interactive computational fluid dynamics. In Volker Bertram & Emilio F. Campana, editor, *18th Numerical Towing Tank Symposium*, Cortona Italy, 28-30 September 2015.
- G D Weymouth and M S Triantafyllou. Global vorticity shedding for a shrinking cylinder. *Journal of Fluid Mechanics*, 702:470–487, 2012.
- G D Weymouth, V Subramaniam, and M S Triantafyllou. Ultra-fast escape maneuver of an octopus-inspired robot. *Bioinspir. Biomim.*, 10(1):016016, feb 2015. doi: 10.1088/1748-3190/10/1/016016. URL <http://dx.doi.org/10.1088/1748-3190/10/1/016016>.
- Gabriel D. Weymouth and M. S. Triantafyllou. Ultra-fast escape of a deformable jet-propelled body. *Journal of Fluid Mechanics*, 721:367–385, 2013.
- M. S. Wibawa, S. C. Steele, J. M. Dahl, D. E. Rival, G. D. Weymouth, and M. S. Triantafyllou. Global vorticity shedding for a vanishing wing. *Journal of Fluid Mechanics*, 695:112–134, 2012.
- Jie-Zhi Wu, Hui-Yang Ma, and Ming-De Zhou. *Vorticity and vortex dynamics*. Springer Science & Business Media, 2007.